Pure Appl. Chem., Vol. 81, No. 1, pp. 45–60, 2009.
doi:10.1351/PAC-CON-08-09-02

Nanometer-scale dynamics of charges generated by radiations in condensed matter*

Akinori Saeki‡ and Seiichi Tagawa

The Institute of Scientific and Industrial Research, Osaka University, 8-1 Mihogaoka, Ibaraki, Osaka 567-0047, Japan

Abstract: The dynamics of short-lived charges generated by pulsed radiations such as electron beam (EB) and photon was investigated to elucidate their reactivity, electronic properties, and spatial behavior on a nanometer scale. Chemical reactions of radical cations (hole) and anions (electron) in condensed matter (organic liquids, polymers, and conjugated materials) occupy an important place in postoptical nanolithography and organic electric devices. The spatiotemporal evolution of charges during geminate ion recombination was measured by a highly improved picosecond (ps) pulse radiolysis and incorporated into a Monte Carlo simulation to clarify the key role of the charges in the formation of latent image roughness of chemically amplified resists (CARs). The dynamics and alternating-current (AC) mobility of transient charge carriers in conjugated materials such as polymer and organic crystals were studied by the combination of microwave conductivity and optical spectroscopies, revealing the potential plausibility for high-performance electric devices. Anisotropy measurement and methodology to resolve the sum of mobility into hole and electron components without electrodes have also been demonstrated.

Keywords: pulse radiolysis; geminate ion recombination; postoptical lithography; conjugated materials; charge carriers.

INTRODUCTION

Nanoscience and nanotechnology have been some of the most famous terminologies in the past several years not only in academic research fields, but also in industrial applications such as cosmetics, health care, lithography, etc. [1]. Regarding the technology to inspect nanometer-scale topology, since a transmission electron microscope was invented by Ernst Ruska and Max Knoll in 1931 [2] and further improvement of spatial resolution had been performed, the human race has gained a direct observation tool to access a nanometer-scale structure that is much smaller than the wavelength of visible light. Other microscopes like an atomic force microscope and scanning tunneling microscope were developed and have served as indispensable tools for the direct observation of ultra-small structure with high resolution on the nanometer scale or less.

Radiations [e.g., α-ray, β-ray, γ-ray, neutron, cosmic ray, charged particle (ion) beam, X-ray, and photon beam] have been used in various fields such as inspection of small structure or element of materials (e.g., X-ray diffraction, microscopes, and spectroscopy), fabrication of nanostructures (e.g., photo/electron beam (EB) lithographies, focused ion beam), improvement or reformation of materials

Pure Appl. Chem.* **81, 1–84 (2009). A collection of invited, peer-reviewed articles by the winners of the 2008 IUPAC Prize for Young Chemists.

‡Corresponding author: Tel.: +81-6-6879-8502; Fax: +81-6-6876-3287; E-mail: saeki-a@sanken.osaka-u.ac.jp

(e.g., curing, crosslink of rubber), production of energy (nuclear reactor), human health care (e.g., cancer therapy, roentgen), and sterilization (e.g., foods, medical instruments). While all applications using the radiations are not covered above, it should be emphasized that the radiations have occupied an important place in nanotechnology as a probe to measure reactions or as a source to generate chemical intermediates.

Although the state-of-the-art microscope technologies provide methods to observe ultra-small structures with high-spatial resolution, their time resolutions have not been enough to investigate the chemical and physicochemical reactions which occur on femto-, pico-, and nanosecond time scale, except for time- and space-resolved fluorescence spectroscopy [3]. With respect to the spectroscopies of bulk materials without spatial resolution, ultra-high time resolution has been achieved with the advent of femto- or attosecond lasers, which enable us to investigate many kinds of chemical reactions.

As for the reactions induced by high-energy EB, since a stroboscopic pulse radiolysis analogous to a pump-probe photolysis was developed in 1970 [4], improvements of the measurement system and investigations on reactivity of chemical intermediates have been conducted worldwide. The simultaneous ability to accompany time and spatial resolutions has not been realized yet for photoabsorption spectroscopy by pulse radiolysis. The author and co-workers have approached a picosecond (ps)- and nanometer-scale reaction by reconstructing a time evolution of spatial distribution of positive and negative charges by measuring and analyzing the kinetic traces of the recombination of these charged species. A liquid alkane was employed as a model compound of polymer. The results were applied to the investigation on the nanometer-scale space-resolved chemical reactions in chemically amplified resists (CARs) which have been used in the mass production of integrated electric circuits. As the feature sizes of circuits shrink, roughness of the topography has emerged as one of the most serious problems in the normal operation of transistors. The author elucidated the formation mechanism of nanometer-scale roughness of latent images and quantified the dependence of roughness on process parameters by using original Monte Carlo simulations. It was clarified for the first time that the nanometer-scale dynamics of the chemical intermediates correlates with and has significant impact on the topography roughness of ultra-small pattern.

In contrast with the "top-down nanotechnology" represented by lithographic techniques, "bottom-up nanotechnology", such as self-assembly and molecular nanoelectronics, has evolved as a major class of research topics in recent years. Considerable effort has been devoted to the development of novel organic materials and their characterizations. There is no doubt that the investigations on nanometer-scale dynamics of charge carriers (i.e., electric conductivity and mobility) are important not only to produce a complete picture of physics and chemistry that occur in the nanometer-scale electronics, but also to improve their performances. The feasibility of such a low-cost, high-efficient, and flexible device has been of great interest for the realization of high-informative ubiquitous society. The author approached nanometer-scale electric conductivity of conjugated materials by using microwave as a probe. The microwave conductivity technique reflects intrinsic charge carrier mobility because this alternating-current (AC) technique does not necessitate an electrode, and thus, the effect of undesired factors such as impurities, structural defects, and strong electric field disturbing thermal motion of charge carriers are minimized.

PICOSECOND- AND NANOMETER-SCALE DYNAMICS OF CHARGES BY PULSE RADIOLYSIS

Over the past decades, pulse radiolysis has served as a useful tool for detailed investigations on chemical kinetics of ultra-fast phenomena initiated by radiation. Since radiation-induced reactions include many of the intermediates that are difficult to be monitored and/or generated substantially through conventional organic chemistry, the research centered around this technique has diversified into various fields, such as radiation chemistry, nuclear engineering, biochemistry, radiotherapy, environmental chemistry, organic chemistry, and lithography. Stroboscopic pulse radiolysis [4] using pulsed radiation

and a probe light pulse, which is known as the pump and probe method in flash photolysis, is appropriate for the direct measurement of the dynamics of short-lived species in ps range and shorter. With the advent of the femtosecond (fs) laser, the present trend in ps pulse radiolysis systems is a combination of the EB linear accelerator (linac) as an irradiation source and fs/ps lasers as probe light. Development of the systems and research studies using them have been performed on a worldwide level [5,6].

Ionizing radiations such as EB and extreme ultraviolet (EUV) have attracted much attention because of its high convergence and potential use as a manufacturing tool of semiconductor devices and nanotechnology-based products. For a full-fledged industrial application of ionizing radiations forthcoming, the basic understanding of both radiation chemical reactions and the spatiotemporal details of the short-lived species generated by irradiation become important. The realization of nanolithography depends on the development of resist materials capable of resolving nanofeatures.

In order to perform highly accurate experiments of ps pulse radiolysis, it is indispensable to develop and improve the measurement system, in terms of time resolution, signal-to-noise (S/N) ratio, and extension of available wavelength of probe. Figure 1 shows the schematic of the pulse radiolysis system based on an L-band linac at the Institute of Scientific and Industrial Research (ISIR), Osaka University. The time resolution is determined by the pulse durations of EB and probe light, time jitter between the electron and probe pulses, and velocity difference of the beam and probe light in a sample (related to length of optical path and refractive index of a sample). As for the pulse width of EB and the time jitter, they were minimized by the development of magnetic pulse compression system [6a] and time-jitter compensation system [6b], respectively. In addition to the development of high time resolution, the expansion of available wavelength range is essential for exploring various kinds of short-lived intermediates and gaining precise pictures of their structure, electrical states, reactivity, and so on. For this purpose, the author and co-workers introduced a new trigger/synchronization circuit and an optical parametric amplifier (OPA) which can tune the wavelength of an fs laser from ultraviolet (UV) to infrared (IR) [7]. An OPA, however, cannot generate a continuum spectrum, but rather only two or three discrete wavelengths at the same time. To overcome this drawback, the author developed further a new system [8] utilizing a stable white light continuum generated by focusing the fundamental oscillation of an fs laser into a sapphire or CaF_2 plate, a high-sensitivity charge-coupled detector (CCD) array, and

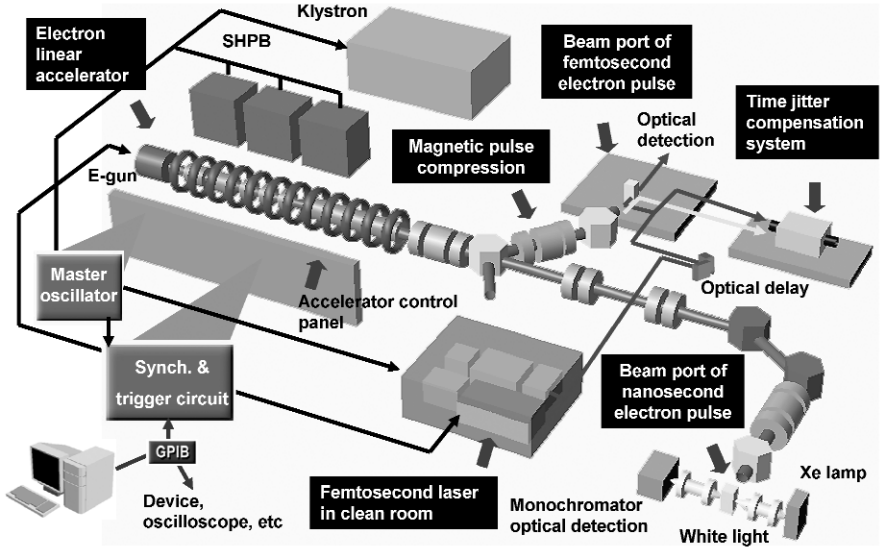

Fig. 1 Schematic of subpico-, pico-, and nano-second pulse radiolysis at ISIR, Osaka University.

double probe pulse technique [9]. The S/N ratio was increased by approximately 30 times in comparison with the previous white light continuum system [10]. These developments to improve the measurement accuracy are very important especially in the pulse radiolysis experiments, due to low repetition rate limited by, for example, linac and data processing and the minimization of radiation damage of a sample.

Using the present system, radiation-initiated chemical reactions in nonpolar liquid were investigated. Low linear energy transfer (LET) radiation, such as high-energy EB, deposits its energy to matrix via ionization and excitation, where most of these events occur independently in the material as shown in Fig. 2a. The ionization gives rise to radical cations ($RH^{\bullet+}$) and electrons (e^-) with excess energy. The electrons with sufficient energy cause further ionization and excitation until they lose their kinetic energies and become thermalized. In an early stage of a chemical reaction, intermediate species such as a radical cation and a thermalized electron exist in a spur that is produced along the trajectory of the incident and secondary electrons. The pair of the parent radical cation and the thermalized electron is called a geminate ion pair. In a nonpolar liquid, most of the geminate ion pairs recombine through the diffusion in the Coulombic field, since most of the thermalized electrons exist in Onsager distance: r_c where the thermal energy is equivalent to the Coulomb potential ($kT = e^2/\varepsilon r_c$). This reaction is referred to as a geminate ion recombination, and considerable effort has been devoted to understanding this reaction both experimentally [11] and theoretically [12]. Figure 2b is indicative of a kinetic trace of geminate ion recombination monitored at 790 nm, which is mainly assigned to radical cation. The solid line is a theoretical curve obtained from the Smoluchowski equation describing diffusion under the Coulombic potential. In contrast to bulk charge recombination, the theoretical fitting of the geminate ion recombination can convert the kinetic decay into time evolution of mutual distance of the radical cations and electrons, due to the inhomogenous reaction in a spur [9b]. As shown in Fig. 2c, the initial distribution function assumed to be exponential with an average distance of 6.6 nm was rapidly changed to a Gaussian-like shape with the extension of the average distance. The same experiment and analysis have been performed as well for liquid aromatics: benzene and reported a narrower distribution function, probably due to more efficient thermalization of electrons produced via ionization [13]. These results and analysis procedures are applied to the simulation of dynamics of chemical intermediates in CARs presented in the next section.

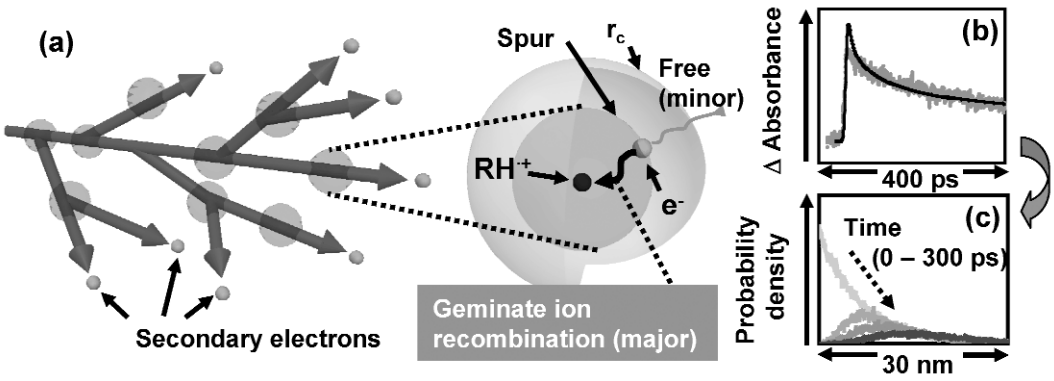

Fig. 2 (a) Illustration of energy-transfer events along the trajectories of low-LET EB. (b) Kinetics of geminate ion recombination in *n*-dodecane monitored at 790 nm by ps pulse radiolysis. The solid line is a theoretical fitting curve. (c) Time evolution of mutual distance of the radical cations and electrons converted from the kinetic analysis of geminate ion recombination.

Not only the geminate ion recombination but also charge transfer from radical ion to scavenger are important primary reactions in radiation chemistry. The author investigated ultra-fast positive charge transfer from solvent radical cation to a cation scavenger: triethylamine (TEA) [14]. On the nanosecond time scale, a few to tens of mM concentration of scavenger are enough to complete the diffusion-controlled charge-transfer reaction. This implies that the charge-transfer reaction in the presence of a high concentration of scavenger must be surveyed on the ps time scale. The kinetics of the radical cation with 0.05–4 M TEA showed an acceleration of the decay caused by the diffusion-controlled scavenging reaction with the rate constant of $7 \pm 3 \times 10^9$ $M^{-1}s^{-1}$; however, accompanying significant decrease of the initial yield of radical cation. This decease could not be explained by a time-dependent rate constant and insufficiency of time resolution. Therefore, the author focused on the charge-transfer reaction without diffusion, i.e., a static quenching which is observed for excited-state quenching in the presence of high-concentrated quencher. The effect that the radical cation *adjacent* to the TEA molecule without diffusion was formulated by consideration of clustering of the TEA molecules, exclusive volume effect, statistical analysis, and Poisson theorem, giving $1 - \exp[-cV(c)]$, where c and $V(c)$ are the concentration of solute and a parameter, respectively. The $V(c)$ has been understood as a constant value representing the volume of a sphere [15]; however, it was proved to be a variable determined by concentration, exclusive volume, and clustering of solutes. The decrease of initial yield of radical cation was well explained by the adjacent effect and direct ionization of solute. This effect was also examined by a configurational-bias Monte Carlo simulation [16] which reproduces a solvent/solute system in liquid phase. Figure 3 shows snapshots of the simulation. The number of solvent molecules adjacent to solute molecule as shown in Fig. 3d was counted, and the probability that the positive charge directly transfers to solute was calculated. The dependence on solute concentration was identical to the statistical model by assuming a reaction radius of 0.5 nm. This radius is reasonable from the viewpoints of molecular sizes of solvent/solute and almost no contribution of electron tunneling across neutral molecules.

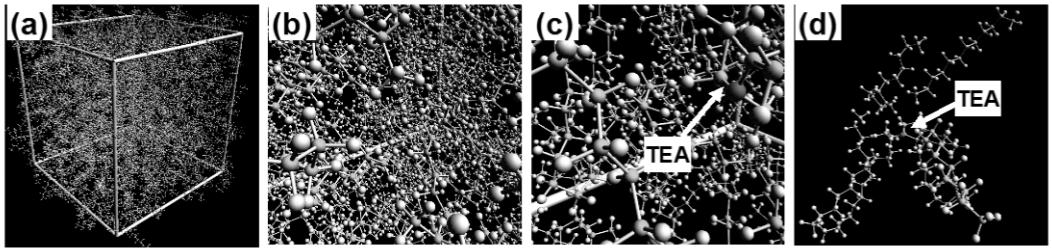

Fig. 3 Reproduction of solvent/solute mixed solution by configurational-bias Monte Carlo simulation. (a) Outer view. (b,c) Inside the box. (d) One solute (TEA) and solvent molecules which are adjacent to each other.

In contrast with the nonpolar solvent, the thermalized electrons generated via ionization in polar solvent such as water [17], alcohol [18], ether [19], and ionic liquid [20] are immediately surrounded by solvent molecules, giving rise to solvated (hydrated) electrons. They have strong and characteristic photo-absorptions in visible or IR region. Among them, tetrahydrofuran (THF), which is one of the typical ethers and has been often used as a good solvent for many aromatics and polymers, has not been well surveyed, in particular on the ps time scale. THF is suitable for the investigation of the reactivity of electrons with photoacid generators (PAGs) [21], which serves as a counter-anion source of acid in CARs, and, thus, it is important to gain more information on the reactivity of solvated/presolvated electrons in THF to shed light on the nature of reaction mechanism of electrons with PAGs or polymeric materials. Biphenyl was used as the scavenger of solvated electrons and its precursor, because it has been widely used in radiation chemistry and the radical anion of biphenyl has strong photo absorption at near-UV and visible wavelength. Picosecond pulse radiolysis in the wavelength range from 400 to 900 nm and discrete 1300 nm was carried out, demonstrating a comprehensive study on the reactivity

of electrons in THF, i.e., formation of biphenyl radical anion, decay of solvated electrons, and decrease of initial yield of solvated electrons were measured and analyzed simultaneously with the same parameter set [22]. A C_{37}, which is defined by the solute concentration to reduce the initial yield of solvated electrons to 1/e, was found to be 87 ± 3 mM. The rate constant of solvated electrons with biphenyl was determined as $5.8 \pm 0.3 \times 10^{10}$ $M^{-1}s^{-1}$. The reaction radius between biphenyl and the solvated electron was found to be 0.44 nm from the rate constant obtained here and the diffusion constants of biphenyl and the solvated electron. At higher concentration of biphenyl (ca. >1 M), further increase of initial yield of biphenyl radical anion (ca. 10 % at 2 M) was observed, accompanying a fast decay component. This fast decay, converging on the flat level found for the low concentration of biphenyl (ca. 200 mM), was explained by the scavenging reaction of precursor of solvated electron by biphenyl and subsequent delayed germinate ion recombination of biphenyl radical anion.

NANOMETER-SCALE DYNAMICS OF PROTON AND ACID IN RESIST POLYMER

Since CAR [23] was deployed in the lithography industries, fabrication of fine pattern has been achieved with high sensitivity. The CARs which utilize photoinitiated acid-catalyzed reaction during postexposure bake (PEB) also have substantial promise for the use in the next-generation lithography industries. The rising demands for higher performance and lower cost for each bit have driven the wavelength of the exposure light source toward shorter from *g* line and *i* line to KrF and ArF excimer lasers. In order to realize a pattern transfer on the scale of, for example, 22 nm, extensive efforts have been devoted to the research and development of postoptical lithography using EUV, 13.5 nm, and EB radiation. As feature sizes shrink, line edge roughness (LER) and line width roughness (LWR) have emerged as some of the most serious problems [24] in the normal operation of transistors and have been subjected to intensive experimental and computational investigations [25] from the viewpoints of physical and chemical properties of resist polymers, process factors such as development condition, and quality of exposure source or electron scattering processes including shot noise. On the stage of the 22-nm technical node, the LWR is required to be less than 1.7 nm, which is almost comparable to the size of a typical resist molecule. To date, an effective methodology not only to meet this requirement but also to be applicable to mass production has not been established. While ionizing exposure sources such as EUV and EB demonstrate the feasibility of ultrafine patterning, it has been reported that the mechanism of acid generation initiated by these ionizing radiations differs from that in photolithography [9,26]. The EUV and EB, of which energies exceed the ionization potential of resists, homogeneously ionize the resist molecules, giving rise to radical cations of mainly resist polymers and ejected electrons. Protons are generated by deprotonation reaction of the radical cations of resist polymers, and counter-anions are produced via dissociative electron attachment between acid generators and the ejected electrons. Therefore, the initial spatial distributions of protons and counter-anions are different from each other.

In order to elucidate the LER formation mechanism and estimate the contribution of the dynamics of chemical intermediates in CARs to LER, the author has performed a Monte Carlo simulation on the basis of ps pulse radiolysis experiments [27]. All of the chemical reactions in CARs exposed to ionizing radiations are listed below, where the monomer unit of poly(4-hydroxystyrene), a typical resist polymer, is denoted as Ph-OH (nonprotected) or Ph-OR (protected). Ionic PAG is represented by a combination of cationic and anionic parts (C^+A^-).

$\text{Ph-OH} \rightarrow \text{Ph-OH}^{\bullet+} + e^-$	(1)	Ionization
$\text{Ph-OH}^{\bullet+} + e^- \rightarrow \text{Ph-OH}^*$	(2)	Recombination
$\text{Ph-OH}^* \rightarrow \text{Ph-OH}$	(3)	Deactivation
$e^- + C^+A^- \rightarrow C^\bullet + A^-$	(4)	Reaction with PAG
$\text{Ph-OH}^{\bullet+} + n(\text{Ph-OH}) \rightarrow \text{Ph-O}^\bullet + n(\text{Ph-OH})H^+$	(5)	Deprotonation

$H^+ + A^- \rightarrow H^+A^-$	(6)	Acid formation
Ph-OR $\rightarrow$ Ph-OH + X PEB	(7)	Deprotection by proton or by acid during
$H^+ + Q \rightarrow QH^+$	(8)	Proton quenching
$H^+A^- + Q \rightarrow QH^+ + A^-$	(9)	Acid quenching

Figure 4 demonstrates the scheme of the simulation from the exposure to EB to the formation of latent image after PEB. It should be noted that all of the above chemical reactions and their spatio-temporal information are involved in the simulation. Base quencher:Q (usually amine which captures and immobilizes proton) is incorporated, because it is used in the actual resist system to enhance LER and spatial resolution. In photolithography, PAG is directly excited, forming acid, and thus the energy deposition and acid formation are identical. However, in EB or EUV lithography, reactions 1–6 would play a key role in the formation of latent images. The correlation between the dynamics of chemical intermediates and formation of LER of latent image was revealed for the first time. Details are presented later in this section.

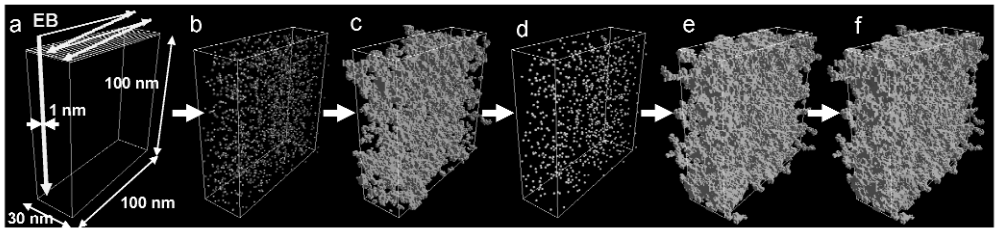

Fig. 4 Nanometer-scale dynamics of proton, anion, and acid in EB-CA resist reproduced by Monte Carlo simulation. (a) Irradiated area. (b) Initial distribution of proton (white) and anion (gray). (c) Latent image catalyzed by proton. (d) Initial distribution of acid before PEB. (e) Latent image catalyzed by acid. (f) Superimposition of (c) and (e).

After the PEB, the latent images are developed by development process in solvent. Figure 5 shows snapshots taken during the development process projected parallel or perpendicular to a substrate [28]. The colors in the figures indicate the percentage of dissolved meshes in the z or y direction. The actual development process has many parameters such as polymer size, solvent size, polymer conformation, dissolution curve, polarity of polymer, etc. However, for simplicity, only the dissolution curve and activation energy of deporotection reaction were incorporated into the simulation to examine the pattern transfer of latent images to the developed feature. A 1-nm cubic mesh was also assumed.

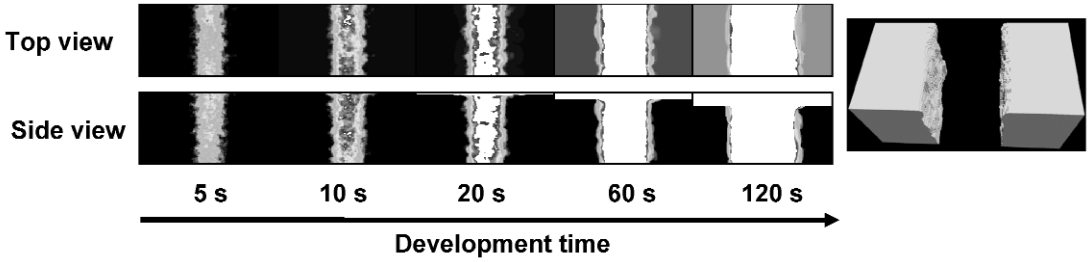

Fig. 5 Snapshots of developed pattern during development process. The gray-scale color indicates the percentage of dissolved meshes in the perpendicular or parallel direction to the substrate. The picture at the right is a 3-dimensional image of developed pattern.

The dependence of LER defined by 3 σ (standard deviation) of edge roughness of latent image is shown in Fig. 6a. Note that the latent image is a pattern feature before development process. With the increase of the line width, which is proportional to the acid diffusion length, the LER was found to be improved and then deteriorated after passing the minimum point. This result is also observed experimentally and can be explained in terms of a smoothing effect and fluctuation in the diffusion length of each acid at the line edge. By increasing the exposure dose or quencher concentration, the curve of the LER line width was shifted to a shorter line width and smaller LER, due to the enhancement of image contrast. Figure 6b indicates the minimum LER found for the LER line width curve for each exposure dose and relative quencher concentration. One would notice that the LER decreased sharply with the exposure dose. The quencher concentration also shows distinguishable LER improvement. However, oversupply of quencher yields a vermiculate latent image, leading to a failure of development. This is suggestive of adequate quencher concentration to form normal line features. On the other hand, the increase of exposure dose enlarges the margin of involved quencher concentration. The minimum LER of the latent image was 9.5 nm for 5 μC cm^{-2} at quencher concentration of 1.0 relative to initial concentration of proton-anion pairs. The LER can be minimized by designing resist formulation and process conditions so that the resists are developed at the minimum point. However, this LER is still eight times higher than the value required in the future nanolithography. In contrast to the small LER observed in non-CA resists [such as polymethyl methacrylate (PMMA) which is used for research purposes], the large LER in the CA resists of EB/EUV can be ascribed to the acid formation process initiated by ionization and the reactions between the acid generators and the low-energy electrons. The mechanism of LER formation elucidated here reveals the origin of LER of latent image, which plays a crucial role in meeting the strict LER requirements for the forthcoming EB/EUV lithography processes.

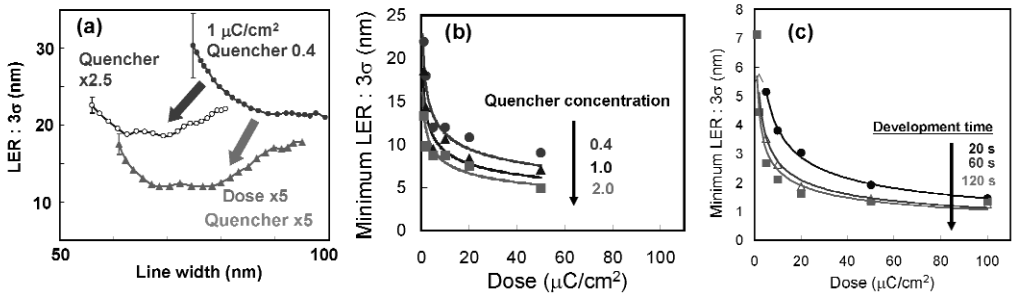

Fig. 6 (a) Correlation between line width (proportional to acid diffusion length) and LER. (b) Dependence of LER of latent images on exposure dose for each relative quencher concentrations. (c) Dependence of minimum LER on exposure dose for each development time.

Although quantitative assessment of LER of latent images was achieved, the actual lithography requires the development process to visualize the pattern. It is of great importance to evaluate the lower bound on LER in EB/EUV lithographies by the present simulation. The LER without development shown in Fig. 6b was overestimated due to the lack of development process and activation energy for deprotection reaction. Figure 6c shows the exposure dose dependence of minimum LER on development time and the increase in line width. LER was reduced significantly with increasing exposure dose and development time, while the slope of the decrease became milder at relatively low values: around 10 μC cm^{-2} and 60 s. The dependences are qualitatively similar to those found in the latent image [27]. An improvement in LER is generally observed at the initial increase of the process parameters, not only for the acid diffusion length (PEB time), but also exposure dose and development time, suggesting that a fine pattern could be achieved by minimal processing. From the fitting curves in Fig. 6c, it is predicted that the LER of less than 1.2 nm required for next-generation lithography is possible by appropriate de-

velopment time, high exposure dose D_{exp} and sufficient acid diffusion length L_{acid}, e.g., D_{exp} = 70 μC cm^{-2} and L_{acid} = 15 nm. It is of great importance that such a small LER was found achievable even though the initial average distance between proton and counter-anion is large (5.6 nm). This reduction is mainly explained by the smoothing effect of acid diffusion, non-zero activation energy, and optimization of the development process. It is expected that the LER is affected in a complex manner, i.e., homogeneity of PAG distribution and polymer characteristics such as configuration, polydispersity, morphology, molecular weight, and interaction with air, vacuum, and substrate. If these factors are taken into consideration, the LER presented here would increase, although its value and dependences remain difficult to be predicted. A preliminary calculation using a 2-nm cubic mesh was carried out, resulting in the increase of LER by a few to several tens of per cent. A randomness of the mesh alignment would increase the LER as well. Significant material factors are expected to appear if the image contrast at the line edge is too low. The change of diffusion coefficient in the catalyzed and uncatalyzed regions might influence the LER. It should, however, be noted that a small LER (<1.2 nm) is achievable by process optimization (electron thermalization distance, PAG concentration, quencher concentration, acid diffusion length, and development parameters) once the resist system can be regarded as an independent 1-nm cubic mesh as assumed here.

DYNAMICS OF CHARGE CARRIERS BY TIME-RESOLVED MICROWAVE CONDUCTIVITY (TRMC)

In modern society, microwave has been used in the wide area of industries such as radar, heating, sterilization, and wireless communication. As for research fields, microwave has served as a probe for microwave spectroscopy, e.g., electron spin resonance (ESR) and nuclear magnetic resonance (NMR), and as a power source for a particle accelerator. Recently, microwave has attracted much attention because of its uniform and selective heating capability, promoting high-efficient and novel chemical reactions. While the recent interests of the application of microwave (wavelength is from 1 mm to 1 m) are in the heating and relating fields as mentioned above, it is applicable to the measurements of chemical reactions and electric properties of materials.

The research presented here is based on the transient change of microwave absorption by charge carriers and/or dipole moments generated by pulse laser or high-energy radiation (mainly an EB or X-ray converted from the EB) [29] as illustrated in Fig. 7. Note that external magnetic field like ESR is not imposed in this technique. The microwave absorption technique was initiated by Biondi et al. in 1959 [30] who measured an electron concentration in gas phase. And then, time-resolved experiments, enhancement of S/N ratio, and extension of measurement dynamic range were realized by improvement of microwave circuit and use of pulsed high-energy radiation. Fessenden et al. at the University of Notre Dame have conducted investigations on dissociative electron attachment in gas phase [31]. Using this microwave technique, Shimamori and Hatano reported electron thermalization process in gas phase and reaction between electron and molecules [32]. The target materials were expanded to transient inter- or intra-molecular dipole moment [33]. The separation of real and imaginary parts of the signals has been discussed in a gas phase [34]. Many investigations regarding an energy loss process [35] and excited states in liquid phase [36] have been performed. Warman et al. at the Delft University of Technology have focused on the charge recombination in hydrocarbons and TiO_2, and charge carrier mobility in conjugated materials [37].

Organic semiconductors represented by amorphous/crystalline films of π- and σ-conjugated polymers, thin films of low-molecular-weight conjugated materials, and supermolecules have attracted much attention for electric devices with flexibility, high efficiency, and novel functionality in the forthcoming ubiquitous information society. Much research and development has been performed from the aspects of not only scientific interests but also the realization of such devices.

As for the characteristics of the organic semiconductors, the mobility of charge carriers provides valuable information in the development of high-performance devices. Generally, the mobility has been

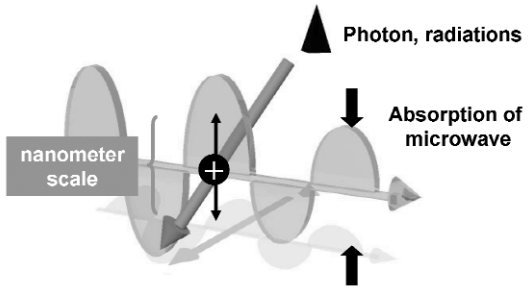

Fig. 7 Schematic of microwave absorption by charge carriers generated by pulsed photon or radiations.

measured by direct-current (DC) technique, e.g., field-effect transistor (FET) and time-of-flight (TOF); however, they are considerably dependent on the film morphology and sample purity like grain boundary, chemical impurities, and structural defects, which are undesired factors hiding the intrinsic charge-transport properties. The interface between the electrodes and the semiconductors causes the problems such as barrier against charge injection and strong electric field, which disturbs the thermal motion of charge carriers. Although the long-range transport property estimated by DC technique is important for the actual electric devices, the intrinsic ability of charge transport cannot always be obtained by DC technique.

To perform direct observation of the drift mobility of charge carriers, free from the disturbance at interfaces such as electrode contacts and domain boundaries, the TRMC technique based on microwave absorption has been developed [37,38]. TRMC, in which the probe is an AC electromagnetic wave, offers the following advantages over DC measurements. (1) As it does not necessitate the fabrication of electrodes in contact with polymers, contact and surface interactions can be avoided. (2) The high frequency (GHz) of microwaves extends the observable region of charge carrier mobility to a very short regime (nanometer scale). Thus, the mobility obtained at end of pulse is not significantly affected by the grain and/or domain boundary conditions. (3) The low magnitude of the electric field (10^{-1}–10^{1} V/cm) makes it possible to observe intrinsic charge-transport phenomena in well-organized and/or highly extended conjugated segments of polymers without perturbing the thermal drift of the charge carriers. Because of these unique properties, the mobilities of polymer matrices obtained by TRMC are typically orders of magnitude higher than those obtained by the DC technique, in which charge migration is dominated by interchain transport and other undesirable factors.

An in situ TRMC-TOS (transient optical spectroscopy) measurement system which can perform flash photolysis-TRMC and TOS with the same experimental geometry was designed and set up [39]. The microwave circuit is intended to separate a real and an imaginary component of the signal. TRMC only gives a conductivity that is a product of charge carrier mobility and its concentration. Therefore, it is essential for the determination of mobility to estimate the carrier concentration by other techniques. From the TOS (or transient absorption spectroscopy, TAS) experiments, we obtain optical density which is a product of molar extinction coefficient, concentration, and optical path. The molar extinction coefficient can be assessed by either pulse radiolysis, γ-ray radiolysis in low-temperature matrix, chemical doping, flash photolysis, or estimation from molecular orbital calculations. As a consequence, the combination of TRMC and TOS gives us a fully experimental estimation of intrinsic charge carrier mobility in organic semiconductors. The obtained results provide not only the potential of the charge carrier mobility in the materials from the viewpoint of application use for organic semiconductor devices, but also shed light on detailed pictures regarding mechanism of formation/decay of the carriers from the transient conductivity signals ranging from nanosecond to millisecond.

Using the TRMC and TOS techniques, the author and collaborators have investigated the charge dynamics in various materials as shown in Fig. 8, such as liquid crystal [40], self-assembled nanotubes [41], σ- [42] and π- [39,43] conjugated polymers (oligomer), DNA [44], organic crystals (or thin film of conjugated molecules) [45], inorganic nanorod [46], and dendrimers [47]. The obtained 9 GHz-AC mobilities of charge carriers are on the orders of 10^{-3}–10^{0} cm^2 $V^{-1}s^{-1}$, which is, in most of the cases, a few orders of magnitude higher than those estimated by DC technique, demonstrating the characteristics of AC mobility and the potential feasibility for the use as efficient organic semiconducting materials. Decay kinetics were found to be sensitive to the film morphology, grain size of thin films, bicontinuous ordering of liquid crystal, and π-stacking distance (e.g., side-chain length of conjugated polymer). The photoconductivity amplitudes were also dependent significantly on the nanometer-scale ordering such as amorphous vs. crystal, random stacking vs. ordered stacking, pristine polymer film vs. film mixed with additive which disturbs the stacking, donor-type materials vs. acceptor-incorporated donor materials, and random-chain vs. rod-like backbone of conjugated polymers. These differences are sometimes hidden in DC measurements by unexpected factors like impurities and film/device conditions.

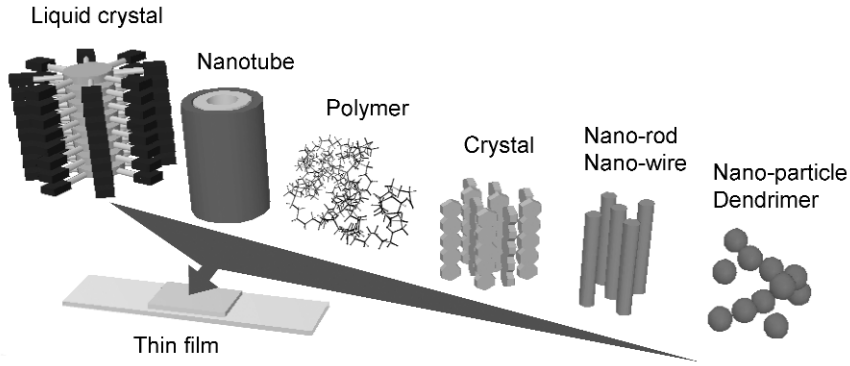

Fig. 8 Semiconducting materials investigated by TRMC and TOS.

Another useful microwave technique is the ability to measure anisotropic conductivity with high-angle resolution without electrodes, just by rotating a sample in a resonant cavity where the direction of microwave electric field is fixed. Self-assembled nanotube showed 10 times higher conductivity along the parallel direction of macroscopically aligned nanotube relative to the perpendicular direction [41b]. For organic semiconducting crystals, anisotropies of 2.3 for rubrene [45a] and 12 for dehydrobenzo[12]annulene [45b] were revealed along more tightly packed directions of the crystalline axis.

The study on single-crystal rubrene [45a] is a good example demonstrating the advantage of the combination of TRMC and TOS measurements. The photoabsorption observed in the wavelength region of 700–1000 nm was assigned to the overlap of radical anion and cation, which was assessed by charge-transfer scheme of nanosecond pulse radiolysis in charge mediator-included solutions. The fast decays of conductivity and photoabsorption transients obeyed second-order kinetics in which the increase of excitation photon density gave the acceleration of these decays. The fluorescence and quantum efficiency of charge carrier generation via excited state decreased with the incident photon density, due to the singlet–singlet exciton annihilation. By comparing long time-scale kinetics of photoabsorption of radical anion and cation, the TRMC mobility estimated to be $(5.2 \pm 0.7) \times 10^{-2}$ cm^2/Vs was separated into ca. 70 % holes and 30 % electron components. This mobility is, however, expected to be the minimum value for several reasons such as much smaller carrier density than those in FET devices, the effect of surface traps, and underestimation of extinction coefficients of charged species in the crystal phase.

The mobility obtained by TRMC is usually higher than or almost equivalent to those assessed by DC techniques; however, semiconductors which give high DC mobility such as single-crystal rubrene resulted in much smaller TRMC mobility. Prins et al. [38i] has reported intramolecular charge carrier mobility along ladder-type polymer chain as high as 600 $cm^2\ V^{-1}s^{-1}$ by analyzing pulse-radiolysis TRMC results using Kubo formula. Not only exploring various kinds of materials and investigating their charge carrier dynamics, but also providing deep insight into the relationship between AC and DC mobility is a remaining challenge.

CONCLUSIONS

Nanometer-scale dynamics of charges was investigated by means of ps pulse radiolysis and TRMC techniques. The author clarified that the dynamics of chemical intermediates has significant impacts on the formation of nano-scale roughness of patterned structures in CARs of postoptical lithography. From the microwave experiments of conjugated materials, the intrinsic mobilities of charge carriers in organic semiconductors were found to be orders of magnitude higher than those reported by conventional DC technique, suggesting the feasibility of the realization of future high-efficient organic electric devices which might overcome the conventional inorganic semiconductors from the viewpoints of cost, flexibility, and their performance.

ACKNOWLEDGMENTS

The author acknowledges Profs. Takahiro Kozawa, Shu Seki, and Yoichi Yoshida for their support of the work. The author also thanks the Japan Society for the Promotion of Science (JSPS) Research Fellowship for Young Scientists. This work was supported in part by a grant-in-aid for scientific research from the sMinistry of Education, Culture, Sports, Science and Technology in Japan (MEXT).

REFERENCES

1. (a) W. A. Goddard III, D. W. Brenner, S. E. Lyshevski, G. J. Iafrate (Eds.). *Handbook of Nanoscience, Engineering, and Technology*, CRC Press, Boca Raton (2003); (b) B. Bhushan (Ed.). *Springer Handbook of Nanotechnology*, Springer Verlag, Berlin (2004).
2. (a) E. Ruska. *Nobel Lectures in Physics* (1986); (b) M. Knoll, J. Kugler. *Nature* **184**, 1823 (1959).
3. (a) M. Merano, S. Sonderegger, A. Crottini, S. Collin, P. Renucci, E. Pelucchi, A. Malko, M. H. Baier, E. Kapon, B. Deveaud, J.-D. Ganieŕe. *Nature* **438**, 479 (2005); (b) W. E. King, G. H. Campbell, A. Frank, B. Reed, J. F. Schmerge, B. J. Siwick, B. C. Stuart, P. M. Weber. *J. Appl. Phys.* **97**, 111101 (2005).
4. (a) M. J. Bronskill, W. B. Taylor, R. K. Wolff, J. W. Hunt. *Rev. Sci. Instrum.* **41**, 333 (1970); (b) C. D. Jonah, M. S. Matheson, J. R. Miller, E. J. Hart. *J. Phys. Chem.* **80**, 1267 (1976).
5. (a) J. F. Wishart, A. R. Cook, J. R. Miller. *Rev. Sci. Instrum.* **75**, 4359 (2004); (b) Y. Muroya, M. Lin, T. Watanabe, G. Wu, T. Kobayashi, K. Yoshii, T. Ueda, M. Uesaka, Y. Katsumura. *Nucl. Instrum. Methods A* **489**, 554 (2002); (c) Y. Aoki, J. Yang, M. Hirose, F. Sakai, A. Tsunemi, M. Yorozu, Y. Okada, A. Endo, X. Wang, I. Ben-Zvi. *Nucl. Instrum. Methods A* **455**, 99 (2000); (d) M. Kawaguchi, K. Ushida, S. Kashiwagi, R. Kuroda, T. Kuribayashi, M. Kobayashi, Y. Hama, M. Washio. *Nucl. Instrum. Methods B* **236**, 425 (2005); (e) J. Belloni, H. Monard, F. Gobert, J.-P. Larbre, A. Demarque, V. De Waele, I. Lampre, J.-L. Marignier, M. Mostafavi, J. C. Bourdon, M. Bernard, H. Borie, T. Garvey, B. Jacquemard, B. Leblond, P. Lepercq, M. Omeich, M. Roch, J. Rodier, R. Roux. *Nucl. Instrum. Methods A* **539**, 527 (2005); (f) J. Yang, T. Kondoh, A. Yoshida, Y. Yoshida. *Rev. Sci. Instrum.* **77**, 043302 (2006); (g) D. A. Oulianov, R. A. Crowell, D. J. Gosztola, I. A. Shkrob, O. J. Korovyanko, R. C. Rey-de-Castro. *J. Appl. Phys.* **101**, 053102 (2007).

6. (a) T. Kozawa, Y. Mizutani, K. Yokoyama, S. Okuda, Y. Yoshida, S. Tagawa. *Nucl. Instrum. Methods A* **429**, 471 (1999); (b) T. Kozawa, Y. Mizutani, M. Miki, T. Yamamoto, S. Suemine, Y. Yoshida, S. Tagawa. *Nucl. Instrum. Methods A* **440**, 251 (2000).
7. A. Saeki, T. Kozawa, S. Kashiwagi, K. Okamoto, G. Isoyama, Y. Yoshida, S. Tagawa. *Nucl. Instrum. Methods A* **546**, 627 (2005).
8. (a) A. Saeki, T. Kozawa, S. Tagawa. *Nucl. Instrum. Methods A* **556**, 391 (2006); (b) A. Saeki, T. Kozawa, K. Okamoto, S. Tagawa. *Jpn. J. Appl. Phys.* **46**, 407 (2007).
9. (a) T. Kozawa, A. Saeki, Y. Yoshida, S. Tagawa. *Jpn. J. Appl. Phys.* **41**, 4208 (2002); (b) A. Saeki, T. Kozawa, Y. Yoshida, S. Tagawa. *Jpn. J. Appl. Phys.* **41**, 4213 (2002).
10. Y. Yoshida, Y. Mizutani, T. Kozawa, A. Saeki, S. Seki, S. Tagawa, K. Ushida. *Radiat. Phys. Chem.* **60**, 313 (2001).
11. (a) J. K. Thomas, K. Johnson, T. Klipper, R. Lowers. *J. Chem. Phys.* **48**, 1608 (1968); (b) M. C. Sauer, C. D. Jonah. *J. Phys. Chem.* **84**, 2539 (1980); (c) C. A. M. van den Ende, L. Nyikos, J. M. Warman, A. Hummel. *Radiat. Phys. Chem.* **15**, 273 (1980); (d) C. D. Jonah. *Radiat. Phys. Chem.* **21**, 53 (1983); (e) S. Tagawa, M. Washio, H. Kobayashi, Y. Katsumura, Y. Tabata. *Radiat. Phys. Chem.* **21**, 45 (1983); (f) S. Tagawa, N. Hayashi, Y. Yoshida, M. Washio, Y. Tabata. *Radiat. Phys. Chem.* **34**, 503 (1989); (g) A. D. Trifunac, M. C. Sauer, C. D. Jonah. *Chem. Phys. Lett.* **113**, 316 (1985); (h) B. C. Le Motais, C. D. Jonah. *Radiat. Phys. Chem.* **33**, 505 (1989); (i) Y. Yoshida, S. Tagawa, M. Washio, H. Kobayashi, Y. Tabata. *Radiat. Phys. Chem.* **34**, 493 (1989); (j) Y. Yoshida, T. Ueda, T. Kobayashi, H. Shibata, S. Tagawa. *Nucl. Instrum. Methods A* **327**, 41 (1993); (k) Y. Yoshida, S. Tagawa, H. Kobayashi, Y. Tabata. *Radiat. Phys. Chem.* **30**, 83 (1987).
12. (a) K. M. Hong, J. Noolandi. *J. Chem. Phys.* **68**, 5163 (1978); (b) K. M. Hong, J. Noolandi. *J. Chem. Phys.* **69**, 5026 (1978); (c) P. P. Infelta, S. J. Rzad. *J. Chem. Phys.* **58**, 3775 (1973); (d) H. A. Schwarz. *J. Chem. Phys.* **55**, 3647 (1971); (e) J. L. Magee. *J. Chem. Phys.* **56**, 3061 (1972); (f) A. L. Nichols, D. Chandler. *J. Chem. Phys.* **87**, 6671 (1987); (g) M. Tachiya. *Radiat. Phys. Chem.* **30**, 75 (1987); (h) W. M. Bartczak, A. Hummel. *J. Chem. Phys.* **87**, 5222 (1987); (i) M. Wojcik, W. M. Bartczak, A. Hummel. *J. Chem. Phys.* **97**, 3688 (1992).
13. K. Okamoto, A. Saeki, T. Kozawa, Yoichi Yoshida, S. Tagawa. *Chem. Lett.* **32**, 834 (2003).
14. A. Saeki, T. Kozawa, Y. Yoshida, S. Tagawa. *J. Phys. Chem. A* **108**, 1475 (2004).
15. (a) I. M. Frank, S. I. Vavilov. *Z. Phys. Chem.* **69**, 100 (1931); (b) A. Weller. *Prog. React. Kinet.* **1**, 187 (1961); (c) H. Boaz, G. K. Rollefson. *J. Am. Chem. Soc.* **72**, 3435 (1950); (d) G. Czapski, E. Peled. *J. Phys. Chem.* **77**, 893 (1973).
16. (a) G. C. A. M. Mooiji, D. Frenkel, B. Smit. *J. Phys.: Condens. Matter* **4**, L255 (1992); (b) M. Lao, J. J. de Pablo, U. W. Suter. *J. Chem. Phys.* **97**, 2817 (1992); (c) J. J. de Pablo, M. Bonnin, J. M. Prausnitz. *Fluid Phase Equilib.* **73**, 187 (1992); (d) R. C. Rizzo, W. L. Jorgensen. *J. Am. Chem. Soc.* **121**, 4827 (1999).
17. (a) E. J. Hart, J. W. Boag. *J. Am. Chem. Soc.* **84**, 4090 (1962); (b) R. K. Wolff, M. J. Bronskill, J. W. Hunt. *J. Chem. Phys.* **53**, 4211 (1970); (c) K. Y. Lam, J. W. Hunt. *Int. J. Radiat. Phys. Chem.* **7**, 317 (1975); (d) C. D. Jonah, J. R. Miller, M. S. Matheson. *J. Phys. Chem.* **81**, 1618 (1977); (e) Y. Gauduel, S. Pommeret, N. Yamada, A. Migus, A. Antonetti. *J. Am. Chem. Soc.* **111**, 4974 (1989); (f) D. M. Bartels, A. R. Cook, M. Mudaliar, C. D. Jonah. *J. Phys. Chem. A* **104**, 1686 (2000); (g) Y. Muroya, M. Lin, G. Wu, H. Iijima, K. Yoshii, T. Ueda, H. Kudo, Y. Katsumura. *Radiat. Phys. Chem.* **72**, 169 (2005); (h) R. Lian, R. A. Crowell, I. A. Shkrob. *J. Phys. Chem. A* **109**, 1510 (2005).
18. (a) S. Arai, M. C. Sauer. *J. Chem. Phys.* **44**, 2297 (1966); (b) M. J. Bronskill, R. K. Wolff, J. W. Hunt. *J. Chem. Phys.* **53**, 4201 (1970); (c) D. Ražem, W. H. Hamill. *J. Chem. Phys.* **82**, 1460 (1978); (d) G. A. Kenney-Wallace, C. D. Jonah. *J. Phys. Chem.* **86**, 2572 (1982); (e) C. Pepin, T. Goulet, D. Houde, J.-P. Jay-Gerin. *J. Phys. Chem.* **98**, 7009 (1994).

19. (a) B. Brockrath, L. M. Dorfman. *J. Phys. Chem.* **77**, 1002 (1973); (b) F. Y. Jou, L. M. Dorfman. *J. Chem. Phys.* **58**, 4715 (1973); (c) A. A. H. Kadhum, G. A. Salmon. *J. Chem. Soc., Faraday Trans. 1* **82**, 2521 (1986); (d) J. A. Dalaire, M. O. Delcourt, J. Belloni. *J. Phys. Chem.* **84**, 1186 (1980); (e) I. B. Martini, E. R. Barthel, B. J. Schwartz. *J. Chem. Phys.* **113**, 11245 (2000); (f) F. Renou, P. Pernot, J. Bonin, I. Lampre, M. Mostafavi. *J. Phys. Chem. A* **107**, 6587 (2003).
20. (a) J. F. Wishart, P. Neta. *J. Phys. Chem. B* **107**, 7261 (2003); (b) J. Grodkowski, P. Neta, J. F. Wishart. *J. Phys. Chem. A* **107**, 9794 (2003).
21. (a) K. Natsuda, T. Kozawa, A. Saeki, S. Tagawa, T. Kai, T. Shimokawa. *Jpn. J. Appl. Phys.* **47**, 4932 (2008); (b) A. Nakano, T. Kozawa, S. Tagawa, T. Szreder, J. F. Wishart, T. Kai, T. Shimokawa. *Jpn. J. Appl. Phys.* **45**, L197 (2006).
22. A. Saeki, T. Kozawa, Y. Ohnishi, S. Tagawa. *J. Phys. Chem. A* **111**, 1229 (2007).
23. (a) H. Ito, C. G. Willson. *Polym. Eng. Sci.* **23**, 1012 (1983); (b) H. Ito. *Adv. Polym. Sci.* **172**, 37 (2005).
24. (a) G. M. Schmid, M. D. Smith, C. A. Mack, V. K. Singh, S. D. Burns, C. G. Willson. *Proc. SPIE* **4345**, 1037 (2001); (b) M. Yoshizawa, S. Moriya. *J. Vac. Sci. Technol. B* **20**, 1342 (2002); (c) W. Hinsberg, F. Houle, M. Sanchez, J. Hoffnagle, G. Wallraff, D. Medeiros, G. Gallatin, J. Cobb. *Proc. SPIE* **5039**, 1 (2003); (d) H. Cao, W. Yueh, B. Rice, J. Roberts, T. Bacuita, M. Chandhok. *Proc. SPIE* **5376**, 757 (2004).
25. (a) S. Mori, T. Morisawa, N. Matsuzawa, Y. Kaimoto, M. Endo, T. Matsuo, K. Kuhara, M. Sasago. *J. Vac. Sci. Technol. B* **16**, 3739 (1998); (b) T. Yamaguchi, K. Yamazaki, H. Namatsu. *J. Vac. Sci. Technol. B* **22**, 2604 (2004); (c) T. Yoshimura, H. Shiraishi, J. Yamamoto, S. Okazaki. *Appl. Phys. Lett.* **63**, 764 (1993); (d) S. Yasin, D. G. Hasko, M. N. Khalid, D. J. Weaver, H. Ahmed. *J. Vac. Sci. Technol. B* **22**, 574 (2004); (e) G. P. Patsis, E. Gogolides, K. Van Werden. *Jpn. J. Appl. Phys., Part 1* **44**, 6341 (2005); (f) G. W. Reynolds, J. W. Taylor. *J. Vac. Sci. Technol. B* **17**, 334 (1999); (g) T. Yamaguchi, H. Namatsu. *J. Vac. Sci. Technol. B* **22**, 1037 (2004); (h) M. Kotera, K. Yagura, H. Niu. *J. Vac. Sci. Technol. B* **23**, 2755 (2005); (i) P. Kruit, S. Steenbrink. *J. Vac. Sci. Technol. B* **23**, 3033 (2005).
26. (a) T. Kozawa, Y. Yoshida, M. Uesaka, S. Tagawa. *Jpn. J. Appl. Phys., Part 1* **31**, 4301 (1992); (b) S. Tagawa, S. Nagahara, T. Iwamoto, M. Wakita, T. Kozawa, Y. Yamamoto, D. Werst, A. D. Trifunac. *Proc. SPIE* **3999**, 204 (2000); (c) T. Kozawa, S. Nagahara, Y. Yoshida, S. Tagawa, T. Watanabe, Y. Yamashita. *J. Vac. Sci. Technol. B* **15**, 2582 (1997); (d) T. Kozawa, A. Saeki, S. Tagawa. *J. Vac. Sci. Technol. B* **22**, 3489 (2004).
27. (a) A. Saeki, T. Kozawa, S. Tagawa, H. B Cao. *Nanotechnology* **17**, 1543 (2006); (b) A. Saeki, T. Kozawa, S. Tagawa, H. B. Cao. *J. Vac. Sci. Technol. B* **24**, 3066 (2006); (c) A. Saeki, T. Kozawa, S. Tagawa, H. B. Cao, H. Deng, M. J. Leeson. *J. Micro/Nanolith. MEMS MOEMS* **6**, 043004-1 (2007)
28. (a) A. Saeki, T. Kozawa, S. Tagawa, H. B. Cao, H. Deng, M. J. Leeson. *Nanotechnology* **19**, 015705 (2008); (b) A. Saeki, T. Kozawa, S. Tagawa, H. B. Cao, H. Deng, M. J. Leeson. *J. Appl. Phys.* **104**, 024303-1 (2008).
29. (a) H. Shimamori. "Microwave conductivity techniques", in *Pulse Radiolysis*, Y. Tabata (Ed.), CRC Press, Boca Raton (1991); (b) J. M. Warman, M. P. de Haas. "Time-resolved conductivity techniques, DC to microwave", in *Pulse Radiolysis*, Y. Tabata (Ed.) CRC Press, Boca Raton (1991); (c) H. Shimamori. "Microwave dielectric absorption studies of photochemical transients", in *Progress in Photochemistry and Photophysics*, Vol. VI, J. F. Rabek (Ed.), CRC Press, Boca Raton (1992).
30. (a) M. A. Biondi, S. C. Brown. *Phys. Rev.* **75**, 1700 (1949); (b) M. A. Biondi, S. C. Brown. *Phys. Rev.* **76**, 1697 (1949); (c) M. A. Biondi. *Rev. Sci. Instrum.* **22**, 500 (1951).
31. (a) R. W. Fessenden, J. M. Warman. *Adv. Chem. Ser.* **82**, 222 (1968); (b) J. M. Warman, R. W. Fessenden, G. Bakale. *J. Chem. Phys.* **57**, 2702 (1972).
32. H. Shimamori, Y. Hatano. *Chem. Phys.* **21**, 187 (1977).

33. (a) R. W. Fessenden, P. M. Carton, H. Paul, H. Shimamori. *J. Phys. Chem.* **83**, 1677 (1979); (b) R. W. Fessenden, P. M. Carton, H. Shimamori, J. C. Scaiano. *J. Phys. Chem.* **86**, 3803 (1982).
34. (a) E. Suzuki, Y. Hatano. *J. Chem. Phys.* **84**, 4915 (1986); (b) E. Suzuki, Y. Hatano. *J. Chem. Phys.* **85**, 5341 (1986).
35. H. Shimamori, T. Sunagawa. *J. Chem. Phys.* **106**, 4481 (1997).
36. R. W. Fessenden, A. Hitachi. *J. Phys. Chem.* **91**, 3456 (1987).
37. (a) M. P. de Hass, J. M. Warman, P. P. Infelta, A. Hummel. *Chem. Phys. Lett.* **31**, 382 (1975); (b) J. M. Warman, M. P. de Hass, M. Grätzel, P. P. Infelta. *Nature* **310**, 306 (1984); (c) R. J. O. M. Hoofman, M. P. de Hass, L. D. A. Siebbeles, J. M. Warman. *Nature* **392**, 54 (1998); (d) J. M. Warman, G. H. Gelinck, M. P. de Haas. *J. Phys.: Condens. Matter* **14**, 9935 (2002).
38. (a) A. M. van de Craats, J. M. Warman, M. P. de Haas, D. Adam, J. Simmerer, D. Haarer, P. Schuhmacher. *Adv. Mater.* **8**, 823 (1996); (b) J. J. Piet, P. N. Taylor, H. L. Anderson, A. Osuka, J. M. Warman. *J. Am. Chem. Soc.* **122**, 1749 (2000); (c) B. Wegewijis, J. Piris, G. Dicker, T. J. Savenije, M. P. de Haas, J. M. Warman. *Synth. Met.* **121**, 1357 (2001); (d) J.-W. van der Horst, P. A. Bobbert, P. H. L. de Jong, M. A. J. Michels, L. D. A. Siebbeles, J. M. Warman, G. H. Gelinck, G. Brocks. *Chem. Phys. Lett.* **334**, 303 (2001); (e) A. M. van de Craats, J. M. Warman. *Adv. Mater.* **13**, 130 (2001); (f) F. C. Grozema, L. D. A. Siebbeles, J. M. Warman, S. Seki, S. Tagawa, U. Scherf. *Adv. Mater.* **14**, 228 (2002); (g) F. C. Grozema, R. J. O. M. Hoofman, L. P. Candeias, M. P. de Hass, J. M. Warman, L. D. A. Siebbeles. *J. Phys. Chem. A* **107**, 5976 (2003); (h) G. Dicker, M. P. de Haas, L. D. A. Siebbeles, J. M. Warman. *Phys. Rev. B* **70**, 045203 (2004); (i) P. Prins, F. C. Grozema, J. M. Schins, S. Patil, U. Scherf, L. D. A. Siebbeles. *Phys. Rev. Lett.* **96**, 146601 (2006); (j) A. C. Pieter, J. Sweelssen, M. M. Koetse, T. J. Savenije, L. D. A. Siebbeles. *J. Phys. Chem. C* **111**, 4452 (2007).
39. (a) A. Saeki, S. Seki, T. Sunagawa, K. Ushida, S. Tagawa. *Philos. Mag.* **86**, 1261 (2006); (b) A. Saeki, S. Seki, Y. Koizumi, S. Tagawa. *J. Photochem. Photobiol. A* **186**, 158 (2007).
40. (a) W.-S. Li, Y. Yamamoto, T. Fukushima, A. Saeki, S. Seki, S. Tagawa, H. Masunaga, S. Sasaki, M. Takata, T. Aida. *J. Am. Chem. Soc.* **130**, 8886 (2008); (b) T. Sakurai, K. Shi, H. Sato, K. Tashiro, A. Osuka, A. Saeki, S. Seki, S. Tagawa, S. Sasaki, H. Masunaga, K. Osaka, M. Takata, T. Aida. *J. Am. Chem. Soc.* **130**, 13812 (2008).
41. (a) Y. Yamamoto, T. Fukushima, Y. Suna, N. Ishii, A. Saeki, S. Seki, S. Tagawa, M. Taniguchi, T. Kawai, T. Aida. *Science* **314**, 1761 (2006); (b) Y. Yamamoto, T. Fukushima, W. Jin, A. Kosaka, T. Hara, T. Nakamura, A. Saeki, S. Seki, S. Tagawa, T. Aida. *Adv. Mater.* **18**, 1297 (2006); (c) Y. Yamamoto, T. Fukushima, A. Saeki, S. Seki, S. Tagawa, N. Ishii, T. Aida. *J. Am. Chem. Soc.* **129**, 9276 (2007).
42. (a) A. Acharya, S. Seki, A. Saeki, Y. Koizumi, S. Tagawa. *Chem. Phys. Lett.* **404**, 356 (2005); (b) A. Acharya, S. Seki, Y. Koizumi, A. Saeki, S. Tagawa. *J. Phys. Chem. B* **109**, 20174 (2005); (c) A. Acharya, S. Seki, A. Saeki, S. Tagawa. *Synth. Met.* **156**, 293 (2006).
43. (a) A. Saeki, S. Seki, Y. Koizumi, T. Sunagawa, K. Ushida, S. Tagawa. *J. Phys. Chem. B* **109**, 10015 (2005); (b) Y. Umemoto, Y. Ie, A. Saeki, S. Seki, S. Tagawa, Y. Aso. *Org. Lett.* **10**, 1095 (2008); (c) A. Saeki, S. Ohsaki, Y. Koizumi, S. Seki, S. Tagawa. *J. Photopolym. Sci. Technol.* **21**, 559 (2008); (d) A. Saeki, S. Ohsaki, S. Seki, S. Tagawa. *J. Phys. Chem. C* **112**, 16643 (2008).
44. R. Yamagami, K. Kobayashi, A. Saeki, S. Seki, S. Tagawa. *J. Am. Chem. Soc.* **128**, 2212 (2006).
45. (a) A. Saeki, S. Seki, T. Takenobu, Y. Iwasa, S. Tagawa. *Adv. Mater.* **20**, 920 (2008); (b) I. Hisaki, Y. Sakamoto, H. Shigemitsu, N. Tohnai, M. Miyata, S. Seki, A. Saeki, S. Tagawa. *Chem.—Eur. J.* **14**, 4178 (2008); (c) H. Imahori, M. Ueda, S. Kang, H. Hayashi, S. Hayashi, H. Kaji, S. Seki, A. Saeki, S. Tagawa, T. Umeyama, Y. Matano, K. Yoshida, S. Isoda, M. Shiro, N. V. Tkachenko, H. Lemmetyinen. *Chem.—Eur. J.* **13**, 10182 (2007); (d) A. Saeki, S. Seki, S. Tagawa. *J. Appl. Phys.* **100**, 023703 (2006).
46. K. Nagashima, T. Yanagida, H. Tanaka, S. Seki, A. Saeki, S. Tagawa, T. Kawai. *J. Am. Chem. Soc.* **130**, 5378 (2008).

47. (a) S. Seki, A. Acharya, Y. Koizumi, A. Saeki, S. Tagawa, K. Mochida. *Chem. Lett.* **34**, 1690 (2005); (b) S. Seki, A. Saeki, A. Acharya, Y. Koizumi, S. Tagawa, K. Mochida. *Radiat. Phys. Chem.* **77**, 1328 (2008).